

# Robust Nonlinear Model Predictive Control of an Autonomous Launch and Recovery System

**DOI:**
10.1109/TCST.2023.3291550

**Document Version**
Final published version

# Robust Nonlinear Model Predictive Control of an Autonomous Launch and Recovery System

Yujia Zhang, Hongbiao Zhao, Guang Li, *Senior Member, IEEE*, Christopher Edwards, *Senior Member, IEEE*, and Mike Belmont

***Abstract*— Launching and recovering a lifeboat from a mother ship is a critical task for rescuing people in high sea states, which can be dangerous to both the mother ship crew and lifeboat personnel. A reliable and efficient control system is crucial to reducing the risk but has not been developed to a mature stage to establish an autonomous launch and recovery system (LARS). A successful manually controlled launch and recovery (L&R) mission relies on empirically assessing the risk and planning the operation ahead of initiating the process. This article proposes a control scheme for the LARS which executes the task in two stages: the L&R risk assessment is conducted in the first stage before hoisting the lifeboat; then in the second stage, input signals are manipulated to accomplish the task once the mission is identified to be safe. We propose a robust tube-based model predictive control (TMPC) law in both stages. It can explicitly consider uncertainties in the LARS model and guarantee constraint satisfaction by bounding possible system trajectories in a predefined tube. Hence degradation of control performance caused by inaccurate system modeling can be minimized to improve the operation safety level of the entire process. The performance of the proposed control scheme is demonstrated by numerical simulations.**

***Index Terms*— Launch and recovery (L&R), model predictive control, safety enhancement.**

## I. Introduction

LAUNCH and recovery (L&R) plays a vital role in the day-to-day operations of working boats and in emergency evacuations. The daily uses of L&R coordinate between offshore vehicles such as embarked aircraft, submersibles, and tenders in support of military and civil tasks, including naval patrols, offshore constructions, and reconnaissance missions [1]. The L&R of lifeboats from mother ships can rescue people in danger and thus has a higher safety standard compared with its routine uses. An efficient lifeboat L&R system relies on accurate judgments and prompt actions of crew members and highly relies on the experiences of the rescue crew. Thus, designing an autonomous control scheme for an L&R system (LARS) is advantageous to mitigating human factors, potentially offering a revolutionary change in L&R executions.

A typical L&R requires the rescue team to empirically evaluate if the mission can proceed safely before initiating the lifeboat hoisting task. This decision can be made more reliably by an autonomous LARS to examine the feasibility of executing the mission in a future period. The feasibility check procedure is the first stage of the LARS control, including the prediction of sea wave magnitudes and the computation of the wave-induced mother ship's motions. The motions are later used as predictable disturbances for the LARS to judge whether it is possible to guarantee a successful completion of the L&R operation. The process will be repeated until a safe window is found out for the execution of L&R. Once the time window is identified, in the following Stage 2, the L&R strap is attached to the link of the lifeboat prior to the identified initiating time; then the hoisting process is accomplished by the LARS control system within the time window. Both stages require the preview information of waves, and thereby the LARS operation is a noncausal control problem.

The main challenge associated with the LARS controller design arises from the influence of inaccurate wave-induced vessel motion predictions. The prediction accuracy has a direct impact on the feasibility issue and influences the execution of L&R, but a highly accurate prediction is not likely available using current technologies. First, the forecast wave profile inevitably involves errors that are transmitted to the mother ship's motion responses. Second, the hydrodynamics of the mother ship can only be approximately computed, which further degrades the motion forecasting precision. Thus, the controller is required to exhibit sufficient robustness to disturbances associated with the LARS, including prediction errors. In addition, practical limitations and constraints, e.g., actuators' torque limits, swing angle constraints, and so on, are imposed on the LARS control scheme. To the best of our knowledge, very few researchers have investigated the LARS control issue with a specific focus on fulfilling these targets. We recently proposed a LARS modeling and robust sliding mode control scheme that manages the hoisting of a lifeboat recovery mission [2]. The method efficiently completes the task with guaranteed stability, but the controller

Manuscript received 1 August 2022; revised 23 January 2023; accepted 7 April 2023. Date of publication 18 July 2023; date of current version 18 August 2023. This work was supported by the Engineering and Physical Sciences Research Council (EPSRC) (Control of Launch and Recovery in Enhanced Sea-States: Part of the Launch and Recovery Co-Creation Initiative) under Grant EP/P023002/1 and Grant EP/P022952/1. Recommended by Associate Editor M. Mammarella. *(Corresponding author: Guang Li.)*

Yujia Zhang, Hongbiao Zhao, and Guang Li are with the Department of Electrical and Electronic Engineering, University of Manchester, M13 9PL Manchester, U.K. (e-mail: yujia.zhang.uom@gmail.com; hongbiao.zhao@postgrad.manchester.ac.uk; guang.li@manchester.ac.uk).

Christopher Edwards and Mike Belmont are with the College of Engineering, Mathematics and Physical Sciences, University of Exeter, EX4 4QF Exeter, U.K. (e-mail: c.edwards@exeter.ac.uk; m.r.belmont@exeter.ac.uk).

Color versions of one or more figures in this article are available at https://doi.org/10.1109/TCST.2023.3291550.

Digital Object Identifier 10.1109/TCST.2023.3291550

cannot explicitly deal with model uncertainties; the swing of the lifeboat is considered but is not suppressed by the control system. In comparison, this article employs a tube-based model predictive control (TMPC) scheme that explicitly copes with the LARS plant-model mismatches and deals with practical restrictions including safety constraints, such as the swing angle. Therefore, the risk of possible collisions between the mother ship and the lifeboat can be reduced.

The applied TMPC is a robust optimization-based control strategy with the guarantee of constraint satisfaction [3]. One TMPC decision variable is the control input of the noise-free nominal model state, solved online based on system dynamics and the initial state. The resulting nominal controller can achieve near-optimality for a high-fidelity model, but it is susceptible to disturbances. Then, the control performance is further improved via another portion of TMPC, to enhance robustness by restricting a bundle of disturbance-involved system trajectories in a tube centered around the nominal state. Regarding the control of the LARS, the tube is obtained from the application of an ancillary controller that penalizes the discrepancy between the real-world LARS trajectories and the nominal model trajectory over time. Hence the safety constraints for all possible states can be satisfied by tightening the constraint set with the predefined tube [3]. The success rate of L&R is thereby greatly increased.

Some additional challenges associated with the LARS TMPC problem and the corresponding solutions provided in this article as follows.

1) The LARS model involves strong nonlinearities introduced by the mother ship's motions. In this sense, the online tractability of the LARS TMPC problem is ensured by utilizing a high-performance optimization framework [4]. The strategy converts the nonlinear predictive control problem into a standard quadratic form by applying the sequential quadratic programming (SQP) strategy. Then, the problem is ultimately solved with a high-performance interior-point method (HPIPM) [5]. Normally, one control step is computed within milliseconds, which can guarantee the computational requirements for real-time implementation of the proposed control algorithm.
2) The investigated LARS is underactuated, which makes the control of the hoisting process and the suppression of the lifeboat swing highly difficult [6]. Hence the adopted TMPC objective mainly penalizes: i) the discrepancy between the current lifeboat position and the expected position; ii) the hoisting velocity $\dot{L}$, as a stable hoisting process and a zero terminal velocity are usually required for a L&R problem; and iii) the lifeboat swing angle or the angular velocity, to avoid possible collisions between the two vessels. Other states of the LARS are mostly constrained but not dominantly penalized.

The contributions of this work and advantageous features of the proposed LARS control scheme as follows.

1) A reliable and automatically controlled LARS is developed in this work. Here the mother ship's hydrodynamics is employed for the prediction of the ship's heave, roll, and sway responses to waves prior to computing the payload motion response to waves. Computation of the hydrodynamics provides a fundamental basis to judge whether the forthcoming L&R execution is safe and then the L&R initiation time is determined accordingly. By contrast, the existing works of offshore operation control schemes mostly assume the mother ship's motions are known to the payload motion computation, which is not realistic in the real world.
2) A LARS TMPC strategy is designed to explicitly consider the optimality, system uncertainties, and constraints. By employing the controller, a relatively high sea state is allowed for L&R missions once the control problem is feasible over an examined period.

The rest of the article is structured as follows. Section II presents the hydrodynamics computation of the mother ship and the modeling of the L&R dynamics. Section III describes the robust TMPC algorithm for the LARS control. Section IV provides simulation results and detailed analysis. Finally, conclusion is drawn in Section V.

## II. Dynamic Model of LARS

The LARS investigated in this article utilizes a stationary davit unit composed of a davit mast, a lifting beam, hydraulic power packs, winches, and a hoist trolley rigged with wire ropes, which are all installed on a mother ship to launch and recover a typical type of lifeboat known as a rigid-hull inflatable boat (RHIB). A double-point lift is employed in the davit system to avoid rotations of the RHIB from the end of the hoist wire; bow or stern lines are used for the same purpose. Swing motions of the RHIB are influenced by the wave-induced motion of the mother ship, which has 6 degrees of freedom (DOF), including heave, sway, surge, roll, pitch, and yaw. The roll angle is denoted as $\alpha$, sway as $y_O$, and heave as $z_O$. The heave and roll movements play a dominant role in influencing the swing of the RHIB while other factors are negligible [7]. Hence the dynamic model of LARS can be considered in a 2-D plane for the purpose of simplification. The diagram is shown in Fig. 1.

Two coordinates are introduced for the LARS modeling: 1) the ship-mounted moving frame $I_S$ and 2) the ground coordinate $I_N$. In the $I_S$ coordinate, the centroid of the mother ship is defined as the origin $\mathcal{O}_S$. The axis $\mathcal{O}_S X_S$ points to the bow (invisible in the 2-D plane) and is perpendicular to the $Y_S - O_S - Z_S$ plane. The earth-fixed inertial reference frame $I_N \triangleq \{O_N, (X_N, Y_N, Z_N)\}$ is developed as a stationary reference, where $Z_N$ is perpendicular to the ground and $X_N$ has the same orientation with $X_S$. Note that the motions of the RHIB are measured based on the $I_S$ coordinate, while the mother ship's motions are observed from the $I_N$ frame.

### A. Mother Ship's Motion Responses to Waves

The frequency response functions $\Phi_w$ for the heave of the ship can be derived analytically [8]. Assuming that the constantly added mass of the cross section is equivalent to the displaced water, the equation of motion in a regular wave with

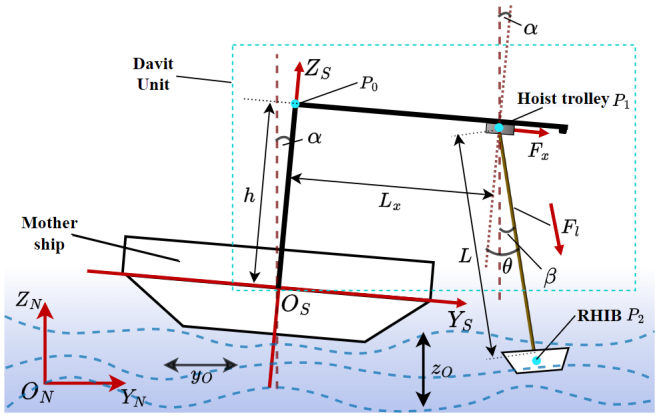


Fig. 1. LARS and reference frames.

amplitude $a$ can be written as

$$2\frac{k_w D}{\omega^2}\ddot{z}_O + \frac{A^2}{k_w B\chi^3\omega}\dot{z}_O + z_O = aF\cos(\varpi t) \tag{1}$$

where $k_w$ is the wavenumber; $\omega$ is the wave frequency; $B$ and $D$ are the breadth and draft of the mother ship, respectively. The parameter $\chi$ is defined as

$$\chi = 1 - F_r\sqrt{k_w L_l}\cos\beta_h \tag{2}$$

in which $L_l$ is the length of the mother ship, and $\beta_h$ is the heading angle. In addition, $F_r$ is the Froude number, such that $F_r = V/(gL_l)^{1/2}$, where $V$ is the forward speed. The frequency of encounter $\varpi$ can be expressed as

$$\varpi = \omega - k_w V\cos\beta_h = \chi\omega. \tag{3}$$

The hydrodynamic damping of the cross section is modeled by the dimensionless ratio between the incident wave amplitude and the diffracted wave amplitude by the following approximation [9]:

$$A = 2\sin\left(\frac{\varpi^2 B}{2g}\right)e^{-\frac{\varpi^2 D}{g}} = 2\sin\left(\frac{1}{2}k_w B\chi^2\right)e^{-k_w D\chi^2}. \tag{4}$$

The driving force $F$ of the mother ship is given by

$$F = \kappa f\frac{2}{k_e L_l}\sin\left(\frac{k_e L_l}{2}\right) \tag{5}$$

with

$$k_e = |k_w\cos\beta_h|. \tag{6}$$

The Smith correction factor $\kappa$ is approximated by

$$\kappa = \exp(-k_e D). \tag{7}$$

*1) Harmonic Oscillator With Sinusoidal Forcing:* A second-order mass-damper-spring system can approximate the decoupled heave $z_O$ and the roll motion $\alpha$ of the mother ship

$$\ddot{\boldsymbol{x}} + 2\xi\omega_n\dot{\boldsymbol{x}} + \omega_n^2\boldsymbol{x} = \frac{F}{m}\sin(\omega t) \tag{8}$$

where $\boldsymbol{x} = [z_O, \alpha]$; $m$ is the system mass. The driving frequency and the natural frequency are denoted by $\omega$ and $\omega_n$, respectively. The variable $\xi$ represents the relative damping ratio, given by

$$\xi = \frac{d}{2}\sqrt{\frac{1}{mk_s}}, \quad \omega_n = \sqrt{\frac{k_s}{m}}. \tag{9}$$

Here $d$ is the system viscous damping coefficient, and $k_s$ is the system elastic damping coefficient.

In this article, we only consider the steady-state solution of the mother ship, which is independent of the initial conditions and only depends on the driving force $F$

$$\boldsymbol{x} = \frac{F}{mZ_m\omega}\sin(\omega t + \varepsilon) \tag{10}$$

with

$$Z_m = \sqrt{(2\xi\omega_n)^2 + \frac{1}{\omega^2}\left(\omega_n^2 - \omega^2\right)^2} \tag{11}$$

$$\varepsilon = \arctan\left(\frac{2\xi\omega_n\omega}{\omega^2 - \omega_n^2}\right) \tag{12}$$

where $Z_m$ is the absolute value of the impedance, and $\varepsilon$ is the phase of the oscillation relative to the driving force. The impedance is the ratio of force $F$ to velocity $\dot{\boldsymbol{x}}$, which represents the degree of the ship's motion when subjected to a sinusoidal force.

*2) Decoupled Computation of the Mother Ship's Natural Periods:* The linear decoupled heave and roll equations are expressed in the center of flotation (CF) [10]

$$\left(m + A_{33}^{\mathrm{CF}}(\omega_3)\right)\ddot{z}_O + \left(B_{33}^{\mathrm{CF}}(\omega_3) + B_{v,33}^{\mathrm{CF}}(\omega_3)\right)\dot{z}_O + C_{33}^{\mathrm{CF}} z_O = 0 \tag{13}$$

$$\left(I_x^{\mathrm{CF}} + A_{44}^{\mathrm{CF}}(\omega_4)\right)\ddot{\alpha} + \left(B_{44}^{\mathrm{CF}}(\omega_4) + B_{v,44}^{\mathrm{CF}}(\alpha_4)\right)\dot{\alpha} + C_{44}^{\mathrm{CF}}\alpha = 0 \tag{14}$$

where the potential coefficients $A_{ii}^{\mathrm{CF}}$ and $B_{ii}^{\mathrm{CF}}$, viscous damping $B_{v,ii}^{\mathrm{CF}}$, spring stiffness $C_{ii}^{\mathrm{CF}}(i = 3, 4)$, and moments inertia $I_x^{\mathrm{CF}}$ are computed in the CF, which is the ship rotation point for a pure rolling motion under the assumption of constant volume displacement. Suppose the natural frequencies are computed in a point far from the CF using the decoupled equations (13) and (14). In this case, the results can be erroneous since the eigenvalues of the decoupled equations depend on the coordinate origin instead of the 6-DOF coupled system. From (13) and (14), it follows that the natural frequencies and periods of heave and roll in the CF are given by the implicit equations

$$\omega_3 = \sqrt{\frac{C_{33}^{\mathrm{CF}}}{m + A_{33}^{\mathrm{CF}}(\omega_3)}}, \quad T_3 = \frac{2\pi}{\omega_3} \tag{15}$$

$$\omega_4 = \sqrt{\frac{C_{44}^{\mathrm{CF}}}{I_x^{\mathrm{CF}} + A_{44}^{\mathrm{CF}}(\omega_4)}}, \quad T_4 = \frac{2\pi}{\omega_4}. \tag{16}$$

Here $T_3$ and $T_4$ are the natural periods of the mother ship in heave and roll; $C_{33}^{\mathrm{CF}} = \rho g A_w$ and $C_{44}^{\mathrm{CF}} = \rho g \bigtriangledown \mathrm{GM}_T$, where $\rho$ denotes the water density; $A_w$ is the lateral area; $\bigtriangledown$ represents the displacement of the mother ship; $\mathrm{GM}_T$ is the transverse metacentric height, and $\mathrm{GM}_L$ is the longitudinal metacentric height.

*3) Heave Response:* Consider the harmonic oscillator

$$\ddot{z}_O + 2\xi\omega_n\dot{z}_O + \omega_n^2 z_O = \omega_n^2 A_a F\cos(\varpi t). \tag{17}$$

The wave amplitude $A_a$ is the driving term. The oscillators have a standard damping ratio $\xi$ and a natural frequency $\omega_n$ such that

$$\xi = \frac{\xi_a^2}{k_s B\mu^3\omega}/2\sqrt{\frac{2k_s D}{\omega^2}} = \frac{\xi_a^2}{B\mu^3\sqrt{8k_s^3 D}} \tag{18}$$

$$\omega_n = \sqrt{\rho g L_l B/\left(m + A_{33}^{\mathrm{CF}}\right)} = \sqrt{g/2D} \tag{19}$$

where $\xi_a$ is the sectional hydrodynamic damping and $\mu$ is the ratio between the frequency of the encounter $\varpi$ and the wave frequency $\omega$. Define the coefficient $f$ as

$$f = \sqrt{(1-k_s D)^2 + \left(\frac{\xi_a^2}{k_s B\mu^3}\right)^2}. \tag{20}$$

Then the driving force $F$ can be written as

$$F = \kappa f\frac{\sin\varsigma}{\varsigma} \tag{21}$$

where $\varsigma = k_e L_l/2$.

Based on (6) and (7), the heave response becomes

$$z_O = A_a\frac{\omega_n^2}{Z_m\varpi}F\cos(\varpi t + \varepsilon) \tag{22}$$

where $Z_m$ and $\varepsilon$ are given by (11) and (12).

*4) Frequency Response Function of the Mother Ship's Roll Angle:* If the roll motion is assumed to be decoupled from other transverse motions, the equation of motion for a roll in regular waves with unit wave amplitude is

$$\left(\frac{T_4}{2\pi}\right)^2 C_{44}\ddot{\alpha} + B_{44}\dot{\alpha} + C_{44}\alpha = M\cos(\varpi t). \tag{23}$$

Here $B_{44}$ is the hydrodynamic damping for the ship; $C_{44} = \rho\bigtriangledown \mathrm{GM}_T$ is the restoring moment coefficient, and

$$B_{44} = 2\zeta_4\left(\frac{T_4}{2\pi}\right)C_{44}. \tag{24}$$

Then an estimate of $M$ as a function of the encounter angle $\beta_e$ is

$$M = \sqrt{\frac{\rho g^2}{\varpi}B_{44}\sin(\beta_e)}. \tag{25}$$

Hence the roll response of the mother ship is formulated as

$$\alpha = \frac{\omega_4^2}{\rho\bigtriangledown \mathrm{GM}_T Z_{m,4}\varpi}M\cos(\varpi t + \varepsilon). \tag{26}$$

*5) Sway Response:* For the sway motion, we can first refer to the mathematical model of ship motions. Then, the ship acceleration equation for the sway motion is given by

$$\dot{v}_s = f_v(\boldsymbol{\nu}) + \frac{\tau_{wv}}{m_v} \tag{27}$$

with

$$f_v(\boldsymbol{\nu}) = -\frac{m_u}{m_v}ur - \frac{d_{v1}}{m_v}v_s - \frac{d_{v2}}{m_v}|v_s|v_s - \frac{d_{v3}}{m_v}v_s^3. \tag{28}$$

Here $\tau_{wv}$ represents the influences from the unmodeled dynamics and external disturbance; $f_v(\boldsymbol{\nu})$ is the high-order hydrodynamic effect. The term $m_v$ denotes the added mass in transverse orientation in the $I_S$ coordinate. The variables $d_{v1}$, $d_{v2}$, and$d_{v3}$ represent the hydrodynamic damping terms. Here the effect of the current is ignored when modeling the motion of the mother ship caused by the waves since: 1) it is challenging to precisely calculate the added mass of the ship and the high-order hydrodynamic parameters; 2) the additional transverse mass of the ship is much larger than the additional longitudinal mass; and 3) the mother ship needs to be adjusted to a position opposite to the direction of the current when the rescue is carried out by releasing the lifeboat following the maritime SOLAS convention described in [11]. The sway motion responses of the mother ship are thereby ignored in this article [10].

### *B. Motions of the Trolley and the Payload in the Body-Fixed Noninertial Frame and the Earth-Fixed Inertial Frame*

The dynamics of the ship-mounted LARS are analyzed using the ship motion responses $z_O$ and $\alpha$. Assume the masses of the hoist trolley and RHIB are $m_1$ and $m_2$. As shown in Fig. 1, $h$ is the height of the lifting beam installed on the mother ship. The trolley displacement along the beam is denoted as $L_x$, where the trolley connects a hoist wire with a length $L$. The swing angle of the RHIB is denoted as $\theta$, which is associated with the L&R operational risk level. For the convenience of establishing the L&R model, we denote the positions of the trolley and the RHIB in the $I_s$ coordinate as $\mathbf{p}_1^S$ and $\mathbf{p}_2^S$

$$\mathbf{p}_1^S = \begin{bmatrix}0 & L_x & h\end{bmatrix}^{\mathrm{T}} \tag{29}$$

$$\mathbf{p}_2^S = \begin{bmatrix}0 & L_x + LS_\theta & h - LC_\theta\end{bmatrix}^{\mathrm{T}}. \tag{30}$$

Here $S_\theta$ and $C_\theta$ represent the functions $\sin\theta$ and $\cos\theta$.

The corresponding velocities of $\mathbf{p}_1^S$ and $\mathbf{p}_2^S$ are

$$\dot{\mathbf{p}}_1^S = \begin{bmatrix}0 & \dot{L}_x & 0\end{bmatrix}^{\mathrm{T}} \tag{31}$$

$$\dot{\mathbf{p}}_2^S = \begin{bmatrix}0\\ \dot{L}_x + \dot{L}S_\theta + LC_\theta\dot{\theta}\\ -\dot{L}C_\theta + LS_\theta\dot{\theta}\end{bmatrix} \tag{32}$$

and their accelerations can be computed by taking the derivatives

$$\ddot{\mathbf{p}}_1^S = \begin{bmatrix}0 & \ddot{L}_x & 0\end{bmatrix}^{\mathrm{T}} \tag{33}$$

$$\ddot{\mathbf{p}}_2^S = \begin{bmatrix}0\\ \ddot{L}_x + \ddot{L}S_\theta + 2\dot{L}C_\theta\dot{\theta} - LS_\theta\dot{\theta}^2 + LC_\theta\ddot{\theta}\\ -\ddot{L}C_\theta + 2\dot{L}S_\theta\dot{\theta} + LC_\theta\dot{\theta}^2 + LS_\theta\ddot{\theta}\end{bmatrix}. \tag{34}$$

Since $\mathbf{p}_i$ $(i = 0, 1, 2)$ is depicted in the body-fixed frame $I_S$, the coordinate transformation formula is introduced in (35) to compute the motions in the earth-centered inertial system $I_N$ as suggested by [7], where

$$\mathbf{p}_i^N = \mathbf{p}_{S-\mathrm{org}}^N + \mathbf{R}_S^N\mathbf{p}_i^S. \tag{35}$$

Here $\mathbf{R}_S^N \in \mathbb{R}^{3\times3}$ is a rotation matrix between $I_S$ and $I_N$ given by (36); $S_\alpha$ and $C_\alpha$ denote $\sin\alpha$ and $\cos\alpha$, respectively; $\mathbf{p}_{S-\mathrm{org}}^N$ is the centroid displacement of the mother ship in the inertial

frame defined by its translational motion $y_O$ and heave motion $z_O$, such that $\mathbf{p}^N_{S-\text{org}} = \begin{bmatrix} 0 & y_O & z_O \end{bmatrix}^{\mathrm{T}}$

$$\mathbf{R}^N_S = \begin{bmatrix} 1 & 0 & 0 \\ 0 & C_\alpha & S_\alpha \\ 0 & -S_\alpha & C_\alpha \end{bmatrix}. \tag{36}$$

The velocity and acceleration of $\mathbf{p}_i (i = 0, 1, 2)$ in the inertial frame are given by (37) according to [12]

$$\dot{\mathbf{p}}^N_i = \dot{\mathbf{p}}^N_{S-\text{org}} + \omega_S \times \mathbf{p}^S_i + \dot{\mathbf{p}}^S_i \tag{37a}$$

$$\ddot{\mathbf{p}}^N_i = \ddot{\mathbf{p}}^N_{S-\text{org}} + \varepsilon_S \times \mathbf{p}^S_i + \ddot{\mathbf{p}}^S_i + \omega_S \times \left(\omega_S \times \mathbf{p}^S_i\right) + 2\omega_S \times \dot{\mathbf{p}}^S_i \tag{37b}$$

where $\omega_S$ is the angular velocity of the mother ship's rolling angle $\alpha$ shown in Fig. 1, such that $\omega_S = \begin{bmatrix} \dot{\alpha} & 0 & 0 \end{bmatrix}^{\mathrm{T}}$; $\varepsilon_S$ is the angular acceleration, where $\varepsilon_S = \begin{bmatrix} \ddot{\alpha} & 0 & 0 \end{bmatrix}^{\mathrm{T}}$.

### C. Dynamic Model of LARS With the Lagrange Equation

A Lagrange equation (38) is employed in the body-fixed $I_S$ frame for dynamic analysis, given that the dynamics can be computed more straightforwardly in the frame attached to the mother ship [13]

$$\frac{d}{dt}\left(\frac{\partial T}{\partial \dot{q}_i}\right) - \frac{\partial T}{\partial q_i} = Q_i \tag{38}$$

where $q_i (i = 1, 2, 3)$ serves as a generalized coordinate, i.e., an independent system state to be controlled. We choose the coordinate vectors for LARS as $q_1 = L_x$, $q_2 = L$, and $q_3 = \theta$ to describe the LARS dynamics. The generalized external forces of the LARS are depicted by $Q_i (i = 1, 2, 3)$, in which the inertial force brought by the relative motion of $I_S$ and $I_N$ is included since $q_i$ is observed in $I_S$. In addition, $T$ is the relative kinetic energy of the LARS, including the kinetic energy of a trolley $T_1$ and the RHIB $T_2$, such that

$$T = T_1 + T_2 = \frac{1}{2}\sum_{i=1}^{2} m_i \left(\dot{\mathbf{p}}^S_i\right)^{\mathrm{T}} \dot{\mathbf{p}}^S_i = \frac{1}{2}(m_1 + m_2)\dot{L}_x^2 + \frac{1}{2}m_2\dot{L}^2 + \frac{1}{2}m_2 L^2\dot{\theta}^2 + m_2\dot{L}\dot{L}_x S_\theta + m_2 L\dot{L}_x\dot{\theta}C_\theta. \tag{39}$$

By substituting (39) into (38), the left side of the Lagrange functions is formulated in terms of each independent state

$$Q_1 = (m_1 + m_2)\ddot{L}_x + m_2 S_\theta \ddot{L} + m_2 C_\theta L\ddot{\theta} + 2m_2 C_\theta \dot{L}\dot{\theta} - m_2 L S_\theta \dot{\theta}^2 \tag{40a}$$

$$Q_2 = m_2 S_\theta \ddot{L}_x + m_2\ddot{L} - m_2 L\dot{\theta}^2 \tag{40b}$$

$$Q_3 = m_2 L C_\theta \ddot{L}_x + m_2 L^2\ddot{\theta} + 2\, m_2 L\dot{L}\dot{\theta}. \tag{40c}$$

The control inputs of the LARS include the tension force $F_l$ along the hoist wire and the trolley driving force $F_x$. Denote the gravitational forces of the trolley and the RHIB as $\mathbf{G}_1$ and $\mathbf{G}_2$. The inertial forces of the trolley and the RHIB are denoted as $\mathbf{F}_1$ and $\mathbf{F}_2$. Then, we utilize $\delta W$ to denote the system's virtual work, which arises from the exerted forces $(F_l,\ F_x)$, the gravitational forces $\mathbf{G}_i (i = 1, 2)$, and the inertial forces $\mathbf{F}_i (i = 1, 2)$. In the generalized coordinates, the generalized external force $Q_i$ is equivalent to $(\delta W)/q_i$.

To compute $Q_i$, we define the virtual work associated with the driving forces as $\delta W_s$, where $\delta W_s$ is given by

$$\delta W_s = F_x \delta L_x + F_L \delta L. \tag{41}$$

Here $\delta L_x$ and $\delta L$ are the variations of $L_x$ and $L$.

Regarding the gravitational virtual work $\delta W_g$, since gravity in the noninertial frame $I_S$ is

$$\mathbf{G}_i = \begin{bmatrix} 0 & -m_i g S_\alpha & m_i g C_\alpha \end{bmatrix}^{\mathrm{T}} \tag{42}$$

by coordinate transformation, $\delta W_g$ can be written as

$$\delta W_g = (m_1 g S_\alpha + m_2 g S_\alpha)\,\delta L_x + m_2 g C_{\theta-\alpha}\delta L - m_2 g L S_{\theta-\alpha}\delta\theta. \tag{43}$$

The virtual work associated with the inertial forces is denoted as $\delta W_s$, which is formulated by

$$\delta W_F = \sum_{i=1}^{2} \mathbf{F}_i \cdot \delta \mathbf{p}^S_i. \tag{44}$$

According to D'Alembert's principle of inertial forces, $\mathbf{F}_i (i = 1, 2)$ arises from: 1) accelerations of the trolley and the RHIB observed in the noninertial frame and 2) relative motions between $I_S$ and $I_N$, where $\mathbf{F}_i$ can be computed by

$$\mathbf{F}_i = -m_i \ddot{\mathbf{p}}^N_i = -m_i \left[\ddot{\mathbf{p}}^N_{S-\text{org}} + \varepsilon_S \times \mathbf{p}^S_i + \ddot{\mathbf{p}}^S_i + \omega_S \times \left(\omega_S \times \mathbf{p}^S_i\right) + 2\omega_S \times \dot{\mathbf{p}}^S_i\right]. \tag{45}$$

Substituting (41), (43), and (44) into (38), the overall virtual work is summarized as

$$\delta W = \left(F_x + m_1 g S_\alpha + m_2 g S_\alpha + f_{L_x}\right)\delta L_x + \left(F_L + m_2 g C_{\theta-\alpha} + f_L\right)\delta L + \left(-m_2 g L S_{\theta-\alpha} + f_\theta\right)\delta\theta. \tag{46}$$

Considering $Q_i = (\delta W)/(\delta q_i), (i = 1, 2, 3)$, the generalized forces are established as

$$Q_1 = F_x - (m_1 + m_2)\ddot{L}_x - (m_1 + m_2)\ddot{y}_O + (m_1 + m_2) g S_\alpha - m_2 S_\theta \ddot{L} + (m_1 + m_2) h\ddot{\alpha} + (m_1 + m_2)\dot{\alpha}^2 L_x - m_2\left(\ddot{\alpha} + \ddot{\theta}\right) C_\theta L - 2m_2\dot{\theta}C_\theta\dot{L} + m_2 S_\theta\left(\dot{\alpha}^2 + \dot{\theta}^2\right) L \tag{47a}$$

$$Q_2 = F_l - m_2\ddot{L} + m_2 C_\theta \ddot{z}_O - m_2 S_\theta \ddot{L}_x - m_2 S_\theta \ddot{y}_O + m_2 g C_{\alpha-\theta} + m_2\left(\dot{\alpha}^2 - \dot{\theta}^2\right) L + m_2\ddot{\alpha}C_\theta L_x - 2m_2\dot{\theta}C_\theta\dot{L}_x + m_2\ddot{\alpha}S_\theta h + m_2\dot{\alpha}^2 S_\theta L_x - m_2\dot{\alpha}^2 C_\theta h \tag{47b}$$

$$Q_3 = -m_2\left(\left(\ddot{\alpha} + \ddot{\theta}\right) L^2 - S_{\alpha-\theta} g L + 2\dot{\theta}\dot{L}L + C_\theta\left(\ddot{L}_x + \ddot{y}_O\right) L + S_\theta \ddot{z}_O L + 2C_\theta\dot{L}_x\dot{L} + \ddot{\alpha}S_\theta L_x L - \ddot{\alpha}C_\theta h L - 2\dot{\theta}S_\theta\dot{L}_x L - \dot{\alpha}^2 C_\theta L_x L - \dot{\alpha}^2 S_\theta h L\right). \tag{47c}$$

Based on (38) and (47), the dynamic model of the LARS is established as (48) with the approximations that $\sin\alpha = \alpha$,

$\cos\alpha = 1$, $\sin\beta = \beta$, $\cos\beta = 1$, $\sin\theta = \theta$, and $\cos\theta = 1$ for small angles

$$\begin{aligned}\ddot{L}_x = &\Big(F_x L - m_1\ddot{y}_O L + m_1 g\alpha L + m_1\ddot{\alpha}hL + m_1\dot{\alpha}^2 L_x L \\ &+ 2m_2\dot{L}_x\dot{L} - F_l\theta L + 2m_2\dot{\theta}^2\theta L^2 + m_2\theta^2\ddot{y}_O L \\ &- m_2\ddot{\alpha}\theta^2 hL - m_2\dot{\alpha}^2\theta^2 L_x L\Big) \Big/ \left(2m_1 L - 2m_2\theta^2 L\right)\end{aligned} \tag{48a}$$

$$\begin{aligned}\ddot{L} = &\Big(-m_1 F_l L + m_2 \\ &\times\Big(\ddot{z}_O L\left(-m_1 + m_2\theta^2\right) \\ &+ L\Big(-m_1\ddot{\alpha}L_x + \theta F_x + m_2 g\theta^2 + 2m_2\dot{\theta}^2\theta^2 L \\ &+ m_2\ddot{\alpha}\theta^2 L_x + m_1 g\left(-1 + \alpha\theta\right) + \dot{\alpha}^2\left(h - L\right) \\ &\times\left(m_1 - m_2\theta^2\right)\Big) \\ &+ 2\dot{L}_x\left(m_2\theta\dot{L} + \dot{\theta}L\left(m_1 - m_2\theta^2\right)\right)\Big)\Big) \\ &\Big/\left(2m_2 L\left(-m1 + m_2\theta^2\right)\right)\end{aligned} \tag{48b}$$

$$\begin{aligned}\ddot{\theta} = &\Big(-F_x L - 4\dot{\theta}\dot{L}L\left(m_1 - m_2\theta^2\right) \\ &- 2\left(m_1 + m_2 - m_2\theta^2\right)\dot{L}_x\dot{L} + \ddot{\alpha}L\left(L + \theta L_x\right) \\ &\times\left(-m_1 + m_2\theta^2\right) + \theta L \\ &\times\Big(F_l - m_1\ddot{z}_O + 2m_1\dot{\theta}\dot{L}_x \\ &- m_1 g + m_1\dot{\alpha}^2 h - 2m_2\dot{\theta}^2 L - m_2 g\alpha\theta + m_2\ddot{z}_O\theta^2 \\ &- 2m_2\theta^2\dot{\theta}\dot{L}_x + m_2 g\theta^2 - m_2\dot{\alpha}^2\theta^2 h\Big)\Big) \\ &\Big/\left(2L^2\left(m_1 - m_2\theta^2\right)\right).\end{aligned} \tag{48c}$$

Clearly, (48) demonstrates that: 1) the LARS states are coupled with the motion predictions of the mother ship computed from the preview wave information and ship hydrodynamics, where the predictions play a vital role in determining the safety of LARS operations; 2) the hoist cable length and the corresponding velocity can be manipulated by controlling the tension force $F_l$; and 3) the payload swing angle $\theta$ is dependent on and determined by both the tension force and the trolley driving force. Hence moving the trolley in the direction of the lifeboat sway is an effective approach to suppress the swing.

Note that all generalized vectors associate with the wave-induced motion responses of the mother ship. Thereby the LARS states can be propagated forward once the heave and roll motion predictions are available. It further implies that the future LARS states and mother ship motions can be predicted by forecasting waves, as the ship motion responses to waves are obtained from (22) and (26).

## III. TMPC-Based L&R Formulation

Efficiently stowing the RHIB and reducing excessive swings are of equal importance for LARS control. Overlong execution time raises the risk of encountering large waves that may cause injuries to lifeboat personnel. Once free from the anti-swing control, the RHIB can move in all directions in response to the hoisting force and the motion of the mother ship. To enhance the reliability of LARS and keep the L&R operation safer, several practical limitations and constraints are imposed on the LARS, e.g., a short execution interval, motors' torque limits, swing angle constraints, and so on. The control objective is to hoist the lifeboat lower down or higher up to reduce the risk of damage from waves subject to the constraints. In this sense, we develop a robust model predictive control scheme that adopts an optimization objective (49) applicable to both stages

$$V^* = \min \int_{t_0}^{t_f} \underbrace{\left((x - x_r)^{\mathrm{T}} Q\,(x - x_r) + u^T Ru\right)}_{\mathbf{f}_0(u(t),t)} dt \tag{49}$$

where $[t_0, t_f]$ is a short time window following the current moment, utilized in Stage 1 to check if the L&R mission can be undertaken safely over the interval. Once the execution of L&R is deemed to be safe during this period, the hoisting can be initiated immediately at the time $t_0$. The terminal time $t_f$ equals $t_0 + N_s T_s$ if the sampling time of the LARS is $T_s$ and the simulation horizon is $N_s$. The state $x = \left[L_x \;\; \dot{L}_x \;\; L \;\; \dot{L} \;\; \theta \;\; \dot{\theta}\right]^{\mathrm{T}}$ in the control problem, is constrained in a compact set $\mathbb{X}$ defined by the practical restrictions of the L&R mechanical system such as the length of the lifting beam. The set $\mathbb{X}$ also accounts for L&R operational safety, e.g., regulating the swing of the RHIB. Note that the state derivative $\dot{x} = \mathbf{f}_c(x, u)$ is twice continuously differentiable.

The stage cost $\mathbf{f}_0(u(t), t)$ in (49) penalizes the discrepancy between the state $x$ and its reference $x_r$, to keep the state trajectories tracking $x_r$ over time. Here we define the state reference $x_r$ as $\left[0_{2\times1} \;\; L_f \;\; 0_{3\times1}\right]^{\mathrm{T}}$, where $L_f$ is the target terminal length. Penalization of the hoisting velocity is also included in $\mathbf{f}_0(u(t), t)$, as it can enable a stable hoisting process and drive the terminal velocity to zero. Some additional penalization terms include: 1) the swing angle $\theta$ or the angular velocity $\dot{\theta}$, since a small swing during L&R execution offers a higher level of safety to the personnel on the RHIB and helps to avoid possible collisions between the two vessels; and 2) the trolley displacement $L_x$ or the corresponding velocity $\dot{L}_x$, to make the motion of the trolley less aggressive, but both $L_x$ and $\dot{L}_x$ are not main penalization terms since the two variables are not directly related to the onboard personnel safety once they are constrained. The weighting matrix $Q$ is chosen to tradeoff between different terms; the weight $R$ is tuned to limit the magnitude of the input signal $u$.

Given the motion prediction errors and plant-model mismatches resulting from unmodeled dynamics, the system equation of the LARS involves unpredictable disturbances that affect the forecasts of its states. Therefore, (49) is hard to be resolved straightforwardly since accurate state predictions are required. Thus, a robust TMPC strategy is employed to convert the optimization problem (49) into two subproblems: 1) a nominal control problem (52) that generates a noise-free central path and 2) an ancillary problem (58) that steers the system trajectories to the central path to eliminate the state discrepancy between the uncertain and nominal states. Hence by tightening the original constraint sets with the boundary of the discrepancy, the proposed TMPC can guarantee the

satisfaction of practical constraints for the LARS. It is also worth noting that both stages of the L&R operations require resolving the two subproblems that jointly formulate the robust LARS controller.

Regarding the implementation of the controller, we first define the nominal LARS model as the derived dynamic model with perfectly-predicted mother ship motions as presented in (48). The predictions are nominal model parameters in the control problem, denoted as $\bar{p} = (\bar{y}_O, \bar{z}_O, \bar{\alpha}_O, \dot{\bar{y}}_O, \dot{\bar{z}}_O, \dot{\bar{\alpha}}_O, \ddot{\bar{y}}_O, \ddot{\bar{z}}_O, \ddot{\bar{\alpha}}_O)$, where the nominal displacements, velocities, and accelerations of the mother ship in response to waves are included. The disturbance-involved mother ship motions are represented by $p = (y_O, z_O, \alpha_O, \dot{y}_O, \dot{z}_O, \dot{\alpha}_O, \ddot{y}_O, \ddot{z}_O, \ddot{\alpha}_O)$. In addition, the nominal state is defined as $z$, the uncertain system state as $x$, and the external bounded disturbances as $\{w|w \in \mathbb{W}\}$ (with $\mathbb{W}$ closed and bounded). Then, the discretized nominal and uncertain L&R dynamics can be described by (50) and (51), respectively, where $z^+$ and $x^+$ denote the successor states of the nominal and uncertain LARS models

$$z^+ = \mathbf{f}(z, v, \bar{p}) \tag{50}$$

$$x^+ = \mathbf{f}(x, u, p) + w. \tag{51}$$

In (50), $\mathbf{f}$ is the mapping from the current states to the successor states solved based on the continuous ordinary differential equation $\mathbf{f}_c$; $v$ is the optimal nominal input computed from a nominal L&R control problem such that $v = [\bar{F}_x, \ \bar{F}_l]^{\mathrm{T}}$. The solution for (50) is denoted by $z(i) = \bar{\phi}(i; z, \mathbf{v})$ at time $i$ with the initial state $z(0)$ and the initial time 0. Here $\mathbf{v}$ in $\bar{\phi}(i; z, \mathbf{v})$ represents the control sequence for the nominal MPC over the horizon $[0, N-1]$ following the current time.

Based on the above definitions, the formulation of the nominal L&R problem is provided by

$$\bar{V}_N^*(z, x_r, v) = \min \sum_{i=0}^{N-1} \ell(\sigma(i), v(i)) \tag{52}$$

$$\text{s.t. } \ell(\sigma(i), v(i)) = \sigma(i)^{\mathrm{T}} Q \sigma(i) + v(i)^{\mathrm{T}} R v(i) \tag{52a}$$

$$\sigma(i) = z(i) - x_r(i) \tag{52b}$$

$$z(i) = \bar{\phi}(i; z, \mathbf{v}) \tag{52c}$$

$$\mathbb{Z} = \kappa_1 \mathbb{X}, \quad \mathbb{V} = \kappa_2 \mathbb{U} \tag{52d}$$

$$z \in \mathbb{Z} \subset \mathbb{X}, \quad v \in \mathbb{V} \subset \mathbb{U}, \ x_r \in \mathbb{X}_r \tag{52e}$$

where the parameters $\kappa_1$ and $\kappa_2$ are utilized to tighten the original constraint sets $\mathbb{X}$ and $\mathbb{U}$; $\mathbb{Z}$ and $\mathbb{V}$ denote the tightened constraint sets lying in the interior of $\mathbb{X}$ and $\mathbb{U}$. Thereby the satisfaction of constraints on the controlled uncertain system can be ensured for all possible disturbance sequences over time [14]. The reference trajectory is bounded in the set $\mathbb{X}_r$.

*Remark 1:* The tightened constraint sets in a linear TMPC problem can be computed by applying the minimal robust positive invariant set theory [15]. While in a nonlinear TMPC problem, the determination of $\mathbb{X}$ and $\mathbb{U}$ is a semiinfinite optimization problem such that the scale parameters $\kappa_1$ and $\kappa_2$ should lie within a discrete subset of $[0, 1]$, but the constraints for the optimization remain infinite dimensional [14]. One way to approximately solve the semiinfinite problem is to apply the Monte-Carlo simulation since a small variation of $\kappa_1/\kappa_2$ does not affect the operational safety as long as the uncertain trajectories mainly stay inside the constraint sets. The strategy can be implemented as follows.

1) Initial choices of the tightened state and control constraints are made such that $\kappa_1, \kappa_2 = 1$.
2) The closed-loop system is simulated using a large sample of disturbance sequences to check the maximum resultant "spread" of system trajectories, say, $2d_i$ $(i = 1, 2, \ldots, 6)$ for a state or control signal.
3) The nominal state and control constraint set is tightened by $d_i$ for each state or control component so that the disturbed trajectories can remain in the interior of the constraint sets. Therefore, the choices of $\kappa_1$ and $\kappa_2$ are neither too conservative nor too aggressive, thus reducing the risk of control performance degradation and violation of constraints.

*Remark 2:* Assume the resultant control sequence of (52) is $\mathbf{v} = [v_{k|0}, v_{k+1|1}, \ldots, v_{k+N-1|N-1}]^{\mathrm{T}}$ from the time $k$. The corresponding optimal state $\boldsymbol{\sigma}$ is $[\sigma_{k+1|1}, \sigma_{k+2|2}, \ldots, \sigma_{k+N|N}]^{\mathrm{T}}$ if $\sigma_{k|0} \triangleq \sigma(0)$. In MPC, only the first control signal $v_{k|0}$ is applied to the LARS at the time $k$ that $v^*(0) \triangleq v_{k|0}$. At the next sampling moment, the current state will be updated by the state measurement at $k+1$ to recompute the control sequences.

*Remark 3:* Assume that the target state $x_r$ is admissible. We outline the method to prove that $z$ can asymptotically converge to the reference trajectory $x_r$ with the nominal MPC law applied.

The convergence can be verified by imposing a terminal cost function $V_f(\sigma(N))$, together with a terminal constraint set $\boldsymbol{\sigma}_f \triangleq \{\sigma(N) \in \boldsymbol{\sigma}_f \subseteq (\mathbb{Z} \ominus \mathbb{X}_r)\}$ as described in [3]. We assume the existence of a positive definite matrix $\{P \mid V_f(\sigma(N)) \triangleq \sigma(N)^{\mathrm{T}} P \sigma(N)\}$ and $P$ is computed from $V_f(\sigma(N+1)) - V_f(\sigma(N)) \leq -\ell(\sigma(N), \kappa_f(\sigma^*_{k+N|N}))$ under a local control law $v_{k+N|N} = \kappa_f(\sigma^*_{k+N|N})$ to make the terminal constraint set $\boldsymbol{\sigma}_f$ invariant. Here $v_{k+N|N}$ can be selected as zero. Thus,

$$\bar{V}_N^*(z, x_r, v) = \min \sum_{i=0}^{N-1} \ell(\sigma(i), v(i)) + V_f(\sigma(N)) \tag{53}$$

which yields an optimal control sequence $\mathbf{v}^* = [v^*_{k|0}, v^*_{k+1|1}, \ldots, v^*_{k+N-1|N-1}]^{\mathrm{T}}$ and an optimal state sequence $\boldsymbol{\sigma}^* = [\sigma(k), \sigma^*_{k+1|1}, \sigma^*_{k+2|2}, \ldots, \sigma^*_{k+N|N}]^{\mathrm{T}}$ if the initial time is $k$. At $k+1$, the control sequence $\mathbf{v}^+ = [v^*_{k+1|1}, v^*_{k+2|2}, \ldots, v^*_{k+N-1|N-1}, \kappa_f(\sigma^*_{k+N|N})]^{\mathrm{T}}$ is suboptimal by the designed control law $\kappa_f(\sigma^*_{k+N|N})$, and therefore,

$$\begin{aligned}
&\bar{V}_N^*\left(z^+, x_r^+, v^+\right) \\
&\leq \sum_{i=1}^{N} \ell(\sigma(i), v(i)) + V_f(\sigma(N+1)) \\
&= \sum_{i=0}^{N-1} \ell\left(\sigma^*_{k+i|i}, v^*_{k+i|i}\right) - \ell\left(\sigma^*_{k|0}, v^*_{k|0}\right) \\
&\quad + \ell\left(\sigma(N), \kappa_f\left(\sigma^*_{k+N|N}\right)\right) + V_f(\sigma(N+1))
\end{aligned}$$

$$= \bar{V}_N^*(z, x_r, v) - \ell\left(\sigma(0), v_{k|0}^*\right) + \underbrace{V_f(\sigma(N+1)) - V_f(\sigma(N)) + \ell\left(\sigma(N), \kappa_f\left(\sigma_{k+N|N}^*\right)\right)}_{\leq 0 \text{ by the above Assumption}} \tag{54}$$

which implies

$$\bar{V}_N^*\left(z^+, x_r^+, v^+\right) - \bar{V}_N^*(z, x_r, v) \leq -\ell\left(\sigma(0), v_{k|0}^*\right). \tag{55}$$

Here $\ell(\sigma(0), v_{k|0}^*) > 0$ for $\sigma(0) \neq 0$ or $v_{k|0}^* \neq 0$.

In addition, to prove the convergence, we assume that there exist $\mathcal{K}_\infty$ functions $c_1$ and $c_f$ [3] satisfying

$$\ell\left(\sigma(0), v_{k|0}^*\right) \geq c_1|\sigma| \tag{56a}$$

$$V_f(\sigma(N)) \leq c_f|\sigma| \tag{56b}$$

for $\forall \sigma \in \mathbb{Z} \ominus \mathbb{X}_r$, then it can be proved following [3] that

$$c_1|\sigma|^2 \leq \bar{V}_N(z, x_r, v) \leq c_2|\sigma|^2 \tag{57}$$

where $c_2 \in \mathcal{K}_\infty$. Since the objective is quadratic that $\bar{V}_N(z, x_r, v) \geq 0$ ($\bar{V}_N(z, x_r, v) = 0$ at equilibrium $\mathbf{O}$ and $\bar{V}_N(z, x_r, v) > 0$ at $\sigma \in (\mathbb{Z} \ominus \mathbb{X}_r) \setminus \mathbf{O}$), the above equation together with (55) implies that the objective function is a Lyapunov function, and $\sigma$ tends to converge to $\mathbf{O}$ over time. Hence the nominal control $v$ asymptotically steers the L&R state $z$ to its admissible reference $x_r$.

*Remark 4:* The constraint set $\boldsymbol{\sigma}_f \triangleq \{\sigma(N) | V_f(\sigma(N)) \leq \Upsilon\}$ can guarantee the feasibility of the successor state if the current state is feasible, where $\Upsilon > 0$. We suppose $\sigma(k)$ is feasible at time $k$ and let $\mathbf{v}^*$ be the optimal control sequence. At time $t+1$, the control sequence $\mathbf{v}^+$ is feasible since $\sigma_{k+N|N}^*$ is in the invariant set $\boldsymbol{\sigma}_f$ and a feasible solution $\kappa_f(\sigma_{k+N|N}^*)$ can always be found to make $\sigma_{k+N+1|N+1}$ in $\boldsymbol{\sigma}_f$.

The disturbed trajectories are required to evolve around the nominal state bounded in a tube. Hence an augmented input $u = [F_x \ F_l]^{\mathrm{T}}$ is introduced to enhance the robustness of the computed nominal controller, solved from an ancillary control problem (58) to steer the uncertain system states toward the nominal trajectory. The objective (58) minimizes the cost of the deviation between the trajectories of the two models $x^+ = \mathbf{f}(x, u, p)$ and $z^+ = \mathbf{f}(z, v, \bar{p})$ [3]. Regarding the penalty weights, we choose their values to be identical to $Q$ and $R$ in the problem (52) for convenience. The weights can be tuned to mitigate the effect of different disturbance sources

$$V_N^*(x, z, u) = \min \sum_{i=0}^{N-1} \ell\left(x(i) - z^*(i), u(i) - v^*(i)\right) \tag{58}$$

$$\text{s.t. } \ell\left(x(i) - z^*(i), u(i) - v^*(i)\right) = \left(x(i) - z^*(i)\right)^{\mathrm{T}} Q \left(x(i) - z^*(i)\right) + \left(u(i) - v^*(i)\right)^{\mathrm{T}} R \left(u(i) - v^*(i)\right) \tag{58a}$$

$$z^*(i) \triangleq \bar{\phi}(i; z, \mathbf{v}), \quad v^*(i) \triangleq v_{i|0} \tag{58b}$$

$$x \in \mathbb{X}, \quad u \in \mathbb{U}. \tag{58c}$$

Here $x(i)$ is the solution of (51) if the control is $u$; $z^*(i)$ is the solution of (50) if the initial state is $z$ and the associated control sequence is $\mathbf{v}$. The initial state $x(0)$ is the current measured state for the disturbed LARS such that $x(0) = [L_{x0} \ 0 \ L_0 \ 0 \ \theta_0 \ 0]^{\mathrm{T}}$. Likewise, the initial nominal state $z(0) \triangleq z_{k|0}$ is obtained from measurement. Moreover, as the state and the control input are constrained in $\mathbb{X}$ and $\mathbb{U}$, the tracking error between the uncertain and reference trajectories is ultimately bounded by an error dynamic set $\Omega \triangleq \mathbb{X} \ominus \mathbb{Z}$, and the uncertain state ultimately stays within the set $x_r \oplus \Omega$ according to Remark 3.

We summarize the control scheme in Fig. 2 following the above discussions, with the implementation details shown in Algorithm 1.

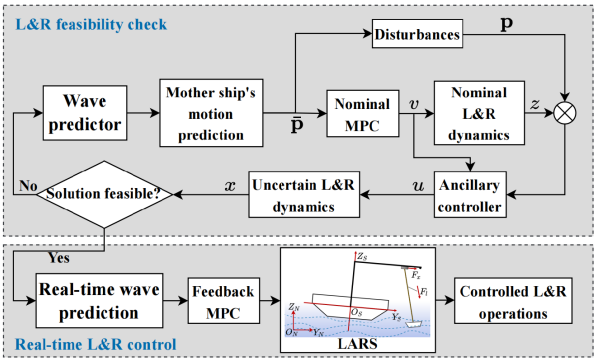


Fig. 2. Control framework of a robust LARS.

**Algorithm 1** Robust Launch and Recovery Control Algorithm

**Result:** The real-time control signal $u$ and state $x$ of a LARS
**Initialization**: mother ship's parameters, initial state, initial choices of the scalar parameters $\kappa_1$ and $\kappa_2$, weighting matrices $Q$ and $R$, constraint sets $\mathbb{X}$ and $\mathbb{U}$
**Sea wave prediction:** Set the current time as 0, forecast short-term wave profiles from $t_0$ seconds after the current time with the deterministic wave prediction algorithm [16];
**Mother ship motion prediction:** Predict the mother ship's motion responses $\bar{p}$ from $t_0$ with the wave predictions and wave hydrodynamics by following Sec. II-A;
**for** $i$ **from** 1 **to** the simulation horizon $N_s$ **do**
  **Nominal controller computation:** Compute the control input $v$ and the state $z$ over $[t_0, t_0 + N_s T_s]$; here the ship motion predictions are applied;
  **Robust MPC law:** From the ancillary control problem, use Monte-Carlo simulations to compute the tube-based robust controllers $u$ and states $x$ over $[t_0, t_0 + N_s T_s]$;
**end**
**Feasibility check:** Check the MPC feasibility for the nominal state;
**if** a feasible solution exists **then**
  Check the maximum resultant spread of system trajectories in Monte-Carlo simulations to update $\kappa_1$ and $\kappa_2$ (see Remark 1);
  Compute $\mathbb{Z} = \kappa_1 \mathbb{X}$, $\mathbb{V} = \kappa_2 \mathbb{U}$;
  Check the feasibility of TMPC for all uncertain states via step 4-7;
  Proceed with step 17 if feasible, or go to step 2;
**else**
  Go to step 2;
**end**
Initiate the L&R operation from $t_0$, and compute the LARS MPC inputs online from $t_0$ to control the operation in real-time.

## IV. Numerical Results

In this section, the JONSWAP wave spectrum [17] is adopted to describe sea states for the L&R mission simulation. The spectral density function is given by

$$S_w(\omega) = 155 \frac{H_s^2}{T_l^4} \omega^{-5} e^{\frac{-944}{T_l^4}\omega^{-4}} \gamma^Y \tag{59}$$

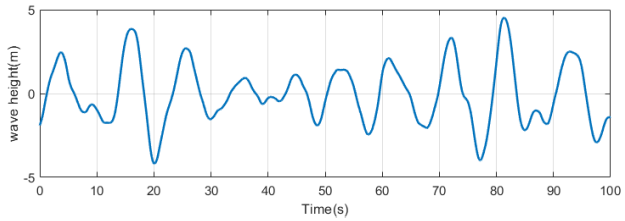


Fig. 3. One Hundred-s of wave profiles.

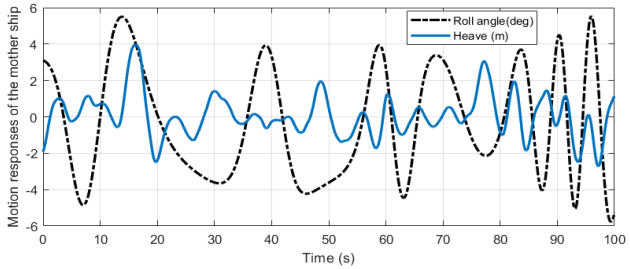


Fig. 4. Mother ship's responses with JONSWAP spectrum.

where $H_s$ is the significant wave height; $T_l$ represents the average wave period [17], and

$$Y = e^{-\left(\frac{0.191\omega T_l - 1}{\sqrt{2}\eta}\right)^2}, \quad \gamma = 3.3 \tag{60}$$

with

$$\eta = \begin{cases} 0.07, & \text{for } \omega \leq 5.24/T_l \\ 0.09, & \text{for } \omega > 5.24/T_l. \end{cases} \tag{61}$$

Here $H_s = 2$ m, $T_l = 40$ s, and $\omega \in (10^{-1.2}, 10^{0.5})$. According to the wave energy spectrum theory, the $n$th wave component possesses the energy of $(1/2)\Delta\omega {A_n}^2$. Here $A_n$ is the amplitude of the $n$th wave component and $\Delta\omega$ is the frequency increment, and $A_n$ is

$$A_n = \sqrt{2S_w(\omega)\Delta\omega}. \tag{62}$$

The wave elevation in the time domain is

$$Z(t) = \sum_{n=1}^{\infty} A_n \cos(\omega_n t + \phi_n). \tag{63}$$

The time-domain wave profile with the frequency varying from $10^{-1.0}$ to $10^{-0.3}$ is shown in Fig. 3.

Suppose the wave incident angle is 60° in a clockwise direction to the bow of the mother ship. The heave and roll motion responses of the mother ship are shown in Fig. 4. The transverse displacement $y_O$ is resulted from the sway motion $v_s$ of the mother ship and thus is trivial according to Section II-A5.

The motion responses are applied as parameters of the nominal LARS model. For a real-world LARS, the motion prediction is computed from sea wave predictions and ship hydrodynamics. The data used to make wave predictions is obtained from scanned $X$-band RADAR images of the sea clutter (operated in short pulse mode) of the region around the vessel out to distances of 1–2 km. These backscatter images are then utilized to create a linear sea model for prediction purposes. Thus, the error in wave profiles arises from both the measurement process and from the assumption of linearity. For prediction times of 30 s ahead in moderate to large seas, the level of accuracy obtained in sea trials is typically 80%–85% [18], [19]. In addition, inaccurate ship hydrodynamics will also bring the model uncertainties as it can influence the computation of motion predictions. The lumped ship motion prediction error is the main source of LARS model uncertainties. We show 40 trajectories of the RHIB's possible motions in Fig. 5. These trajectories evolve around the nominal trajectory (solid lines). Trajectories from Monte-Carlo simulations (dashed and dotted lines) show the robustness of the controller. The first 5 s of the mother ship motion responses is utilized to determine if the control problem is feasible to safely proceed with the L&R operations. Note that choosing a larger slot might include large waves during the time window which makes the L&R problem infeasible. On the other hand, if the hoisting time is designed to be too short, it can arouse large swing angles and possibly very high hoisting velocities according to the L&R system dynamics. For the weighting matrices, we choose $Q = \text{diag}(0, 0.2, 1, 1, 0, 0.5)$ and $R = \text{diag}(3 \times 10^{-5}, 5 \times 10^{-5})$. The rest of the LARS parameters and controller settings are shown in Table I.

TABLE I
PARAMETERS OF THE LARS

| Notation | Value | meaning |
|---|---|---|
| $T_s$ | 0.1s | sampling interval |
| $N_s$ | 50 | simulation horizon |
| $N$ | 20 | prediction horizon |
| $L_l$ | 65 m | length of the ship |
| $B$ | 15 m | width of the ship |
| $D$ | 3.5 m | draught of the ship |
| $m_1$ | 350 kg | mass of the trolley |
| $m_2$ | 695 kg | mass of load-bearing RHIB |
| $g$ | 9.81m/s$^2$ | gravitational acceleration |
| $h$ | 10 m | height of the beam |
| $L_{x0}$ | 10 m | initial trolley position |
| $\dot{L}_{x0}$ | 0 m/s | initial trolley velocity |
| $L_0$ | 10 m | initial length of the hoist wire |
| $\dot{L}_0$ | 0 m/s | initial velocity of the hoist wire |
| $\beta_0$ | 0 deg | initial swing angle |
| $\dot{\beta}_{x,0}$ | 0 deg/s | initial angular velocity |
| $L_f$ | 3m | terminal length of the hoist wire |
| $\dot{L}_f$ | 0 m/s | terminal velocity of the hoist wire |
| $[\bar{F}_{x\,min}\ \bar{F}_{x\,max}]$ | $[-3\times10^4,\ 3\times10^4]$N | range of $\bar{F}_x$ |
| $[\bar{F}_{l\,min}\ \bar{F}_{l\,max}]$ | $[-3\times10^4,\ 3\times10^4]$N | range of $\bar{F}_l$ |
| $[\bar{L}_{x\,min}\ \bar{L}_{x\,max}]$ | $[0,\ 10]$m | range of $\bar{L}_x$ |
| $[\dot{\bar{L}}_{min}\ \dot{\bar{L}}_{max}]$ | $[-4,\ 4]$m/s | range of $\dot{\bar{L}}_x$ |
| $[\bar{\theta}_{min}\ \bar{\theta}_{max}]$ | $[-5,\ 5]$deg | range of $\bar{\theta}$ |

The computation of the TMPC inputs and the corresponding states employs the high-performance optimization framework *acados* to ensure the real-time implementation, as each control step can be performed in milliseconds [4]. Given that each receding-horizon subproblem of MPC is a nonlinear optimal control problem (OCP), the solver can discretize the OCP into a nonlinear programming (NLP) formulation with multiple-shooting discretization [20]. Then, the NLP can be converted into a standard quadratic form using the SQP strategy [21]. The quadratic problem is approximately solved by a Ricatti-based interior-point strategy using the recently developed HPIPM [5].

The nominal trolley driving force $\bar{F}_x$ and the nominal tension force $\bar{F}_l$ are shown in Fig. 6. The resultant control

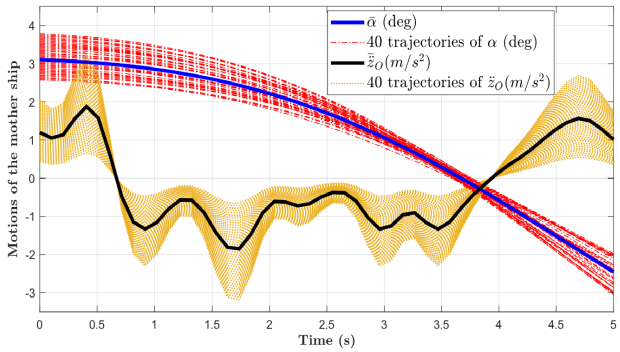


Fig. 5. Predictions of the mother ship's roll angle and heave acceleration responses and 40 trajectories of uncertainty-involved responses.

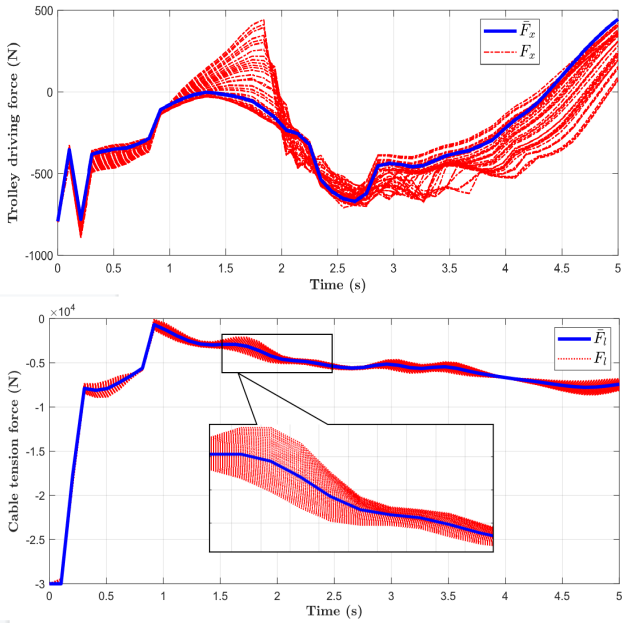


Fig. 6. Forty trajectories of trolley driving forces ($F_x$) and tension forces ($F_l$) and the corresponding nominal control inputs.

signal $\bar{F}_l$ steers the RHIB to the target position during the specified time slot subject to constraints; $\bar{F}_l$ together with $\bar{F}_x$ manipulates the swing of the RHIB. The magnitude of $\bar{F}_x$ is relatively small as the friction between the trolley and the lifting beam is trivial, and the scale of the predicted rolling angle leads to a much smaller trolley acceleration compared with the acceleration of the payload. If the prediction errors are considered, the control inputs (a set of dotted lines in Fig. 6) utilize the solution from the ancillary controller (58) to drive the uncertain trajectories close to the nominal state. The results show that the tension force constraints are active at the beginning.

Motion responses of the LARS are shown in Figs. 7–9 utilizing the obtained control inputs. Fig. 7 shows the changes in the trolley position to suppress the swing of the RHIB. Here the penalization coefficients of the terms $|L_x - \bar{L}_x|$ and $|\dot{L}_x - \dot{\bar{L}}_x|$ in the ancillary control problem are set to be small, thus having negligible impacts on the position tracking performance of the RHIB. In this sense, the discrepancies between the trolley position and velocity between the nominal and uncertain trajectories can be observed. Fig. 8 shows the length of the hoist wire and the corresponding velocity.

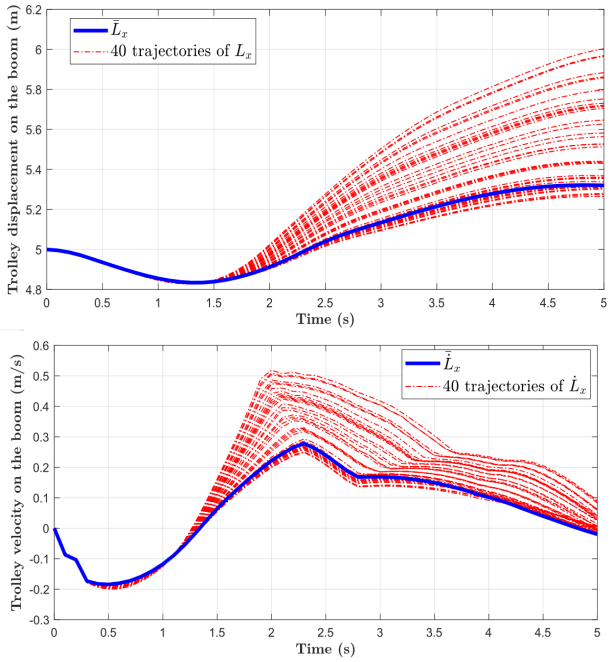


Fig. 7. Forty trajectories of trolley position and velocity on the lifting beam ($L_x$, $\dot{L}_x$) and the corresponding nominal position and velocity.

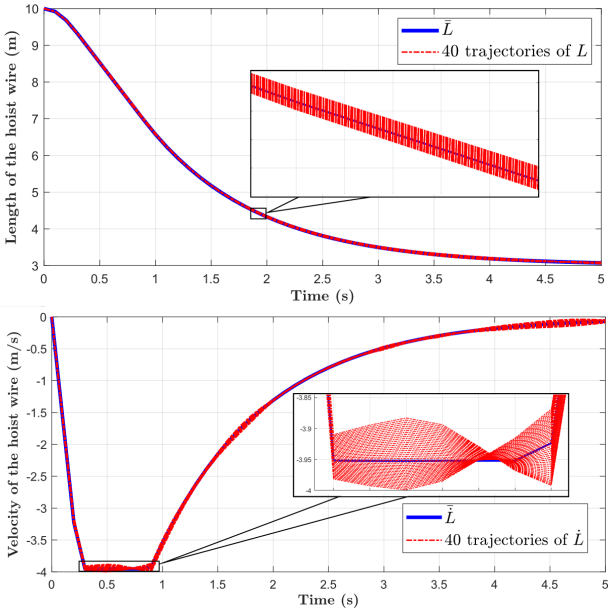


Fig. 8. Forty trajectories of hoist wire's length and velocity ($L$, $\dot{L}$) and the corresponding nominal length and velocity.

Regarding their constraints, the scalar tuning parameter of the state $\kappa_1$ is designed as 0.988 via Monte-Carlo simulations, and the nominal constraints for the cable length and the velocity are thereby tightened to the sets $[\kappa_1 \bar{L}_{\min}\ \kappa_1 \bar{L}_{\max}]$ and $[\kappa_1 \dot{\bar{L}}_{\min}\ \kappa_1 \dot{\bar{L}}_{\max}]$, respectively. Hence the constraints for the cable velocity are active during $[0.3, 0.8]$ s. It is also remarkable that the position of the RHIB keeps tracking the target terminal position $L_f$, which is achieved during the required time period. The terminal velocity approaches zero to stabilize the motion of the hoisted RHIB. Furthermore, despite the existence of minor discrepancies between the nominal and uncertain trajectories, the controller maintains the uncertain system states in a reasonable neighborhood of the reference

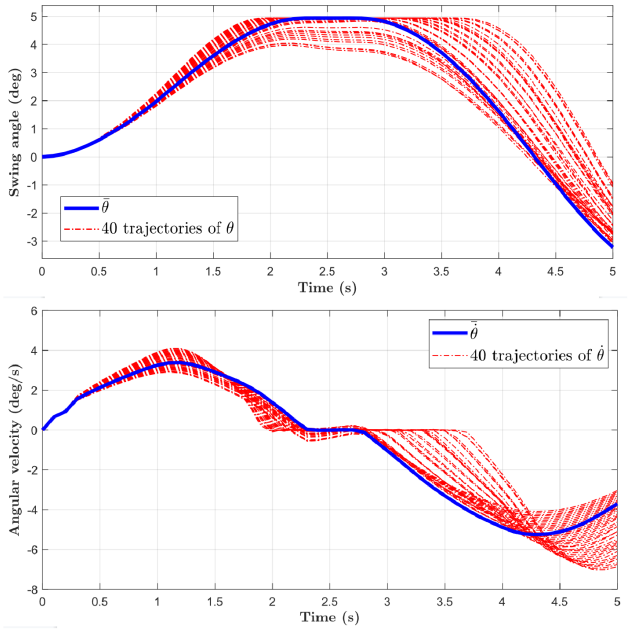


Fig. 9. Forty trajectories of swing angle and angular velocity ($\theta$, $\dot{\theta}$) and the corresponding nominal angle and angular velocity.

trajectory since the impact of model uncertainties is minimized via the ancillary control objective. Therefore, the computed control action is not inclined to be conservative.

Fig. 9 shows the swing angle and angular velocity responses using the nominal and uncertain system dynamics. The nominal value of the swing angle is controlled within its safety constraints $[\kappa_1\bar{\theta}_{\min}\ \kappa_1\bar{\theta}_{\max}] = [-4.94°,\ 4.94°]$, indicating the hoist trolley is moved in the direction of lifeboat swing to counteract the swing. With model uncertainties involved, the system trajectories are regulated to evolve around the nominal state, where all trajectories satisfy the state constraints $[-5°,\ 5°]$ to avoid the possibility of collisions brought by overlarge swings. The robustness of the LARS thereby can be guaranteed, which acts as an additional safety feature and thus the operation can proceed securely. Note that in the LARS TMPC problem, the average simulation time for each MPC loop is 4.2 ms. As the feasibility check is completed in prior to the initiation time of L&R operations, the online tractability is guaranteed.

## V. Conclusion

A robust TMPC scheme tailored for an offshore LARS is proposed in this article. Control of the LARS consists of two stages. The controller feasibility is checked in Stage 1 to examine whether the L&R can proceed securely. Once a feasible solution is found, the controller executes the hoisting to accomplish the L&R mission in Stage 2. In this case, even in a relatively high sea state, it is possible to undertake the L&R mission with the proposed controller applied. In each stage, the system robustness against disturbances can be guaranteed by restricting the LARS uncertainties in a tube centered around a nominal trajectory free of disturbances. To further enhance the safety of the execution, operational limits of the L&R mechanical system are fully considered to protect the LARS, and the likelihood of overlarge payload swinging is reduced by penalizing the angular velocity. Moreover, online tractability is demonstrated despite the fact that the LARS dynamics are profoundly nonlinear. The performance may be further improved by investigating the 3-D modeling and control of the LARS in the future.

## References

[1] E. I. Sarda and M. R. Dhanak, "A USV-based automated launch and recovery system for AUVs," *IEEE J. Ocean. Eng.*, vol. 42, no. 1, pp. 37–55, Jan. 2017.

[2] Y. Zhang, C. Edwards, M. Belmont, and G. Li, "Modeling and sliding-mode control for launch and recovery system in predictable sea states with feasibility check for collision avoidance," *IEEE Trans. Control Syst. Technol.*, vol. 30, no. 6, pp. 2658–2671, Nov. 2022.

[3] J. B. Rawlings, D. Q. Mayne, and M. Diehl, *Model Predictive Control: Theory, Computation, and Design*, vol. 2. Madison, WI, USA: Nob Hill Publishing, 2017.

[4] R. Verschueren et al., "acados—A modular open-source framework for fast embedded optimal control," *Math. Program. Comput.*, vol. 14, pp. 147–183, Mar. 2022.

[5] G. Frison and M. Diehl, "HPIPM: A high-performance quadratic programming framework for model predictive control," *IFAC-PapersOnLine*, vol. 53, no. 2, pp. 6563–6569, 2020.

[6] Y. Qian, Y. Fang, and B. Lu, "Adaptive repetitive learning control for an offshore boom crane," *Automatica*, vol. 82, pp. 21–28, Aug. 2017.

[7] Y. Fang, P. Wang, N. Sun, and Y. Zhang, "Dynamics analysis and nonlinear control of an offshore boom crane," *IEEE Trans. Ind. Electron.*, vol. 61, no. 1, pp. 414–427, Jan. 2014.

[8] J. J. Jensen, A. E. Mansour, and A. S. Olsen, "Estimation of ship motions using closed-form expressions," *Ocean Eng.*, vol. 31, no. 1, pp. 61–85, Jan. 2004.

[9] Y. Yamamoto, N. Imoto, and S. Machida, "Amplitude squeezing in a semiconductor laser using quantum nondemolition measurement and negative feedback," *Phys. Rev. A, Gen. Phys.*, vol. 33, no. 5, pp. 3243–3261, May 1986.

[10] T. I. Fossen, *Handbook of Marine Craft Hydrodynamics and Motion Control*. Hoboken, NJ, USA: Hoboken, NJ, USA: Wiley, 2011.

[11] I. Solas, "International convention for the safety of life at sea (SOLAS)," Int. Maritime Org., London, U.K., 2002.

[12] T. I. Fossen and O.-E. Fjellstad, "Nonlinear modelling of marine vehicles in 6 degrees of freedom," *Math. Model. Syst.*, vol. 1, no. 1, pp. 17–27, Jan. 1995.

[13] B. Lu, Y. Fang, J. Lin, Y. Hao, and H. Cao, "Nonlinear antiswing control for offshore boom cranes subject to ship roll and heave disturbances," *Autom. Construct.*, vol. 131, Nov. 2021, Art. no. 103843.

[14] D. Q. Mayne, E. C. Kerrigan, E. J. van Wyk, and P. Falugi, "Tube-based robust nonlinear model predictive control," *Int. J. Robust Nonlinear Control*, vol. 21, no. 11, pp. 1341–1353, Jul. 2011.

[15] K. I. Kouramas, S. V. Rakovic, E. C. Kerrigan, J. C. Allwright, and D. Q. Mayne, "On the minimal robust positively invariant set for linear difference inclusions," in *Proc. 44th IEEE Conf. Decis. Control*, Dec. 2005, pp. 2296–2301.

[16] L. Abusedra and M. R. Belmont, "Prediction diagrams for deterministic sea wave prediction and the introduction of the data extension prediction method," *Int. J. Shipbuilding Prog.*, vol. 58, no. 1, pp. 59–81, 2011.

[17] K. Hasselmann et al., "Measurements of wind-wave growth and swell decay during the joint north sea wave project (JONSWAP)," *Deutschen Hydrographischen Zeitschrift*, vol. 8, pp. 1–95, Jan. 1973.

[18] M. Al-Ani, M. Belmont, and J. Christmas, "Sea trial on deterministic sea waves prediction using wave-profiling radar," *Ocean Eng.*, vol. 207, Jul. 2020, Art. no. 107297.

[19] M. Al-Ani, J. Christmas, M. R. Belmont, J. M. Duncan, J. Duncan, and B. Ferrier, "Deterministic sea waves prediction using mixed space–time wave radar data," *J. Atmos. Ocean. Technol.*, vol. 36, pp. 833–842, 2019.

[20] H. G. Bock and K. J. Plitt, "A multiple shooting algorithm for direct solution of optimal control problems," *IFAC Proc. Volumes*, vol. 17, no. 2, pp. 1603–1608, Jul. 1984.

[21] C. Büskens and H. Maurer, "SQP-methods for solving optimal control problems with control and state constraints: Adjoint variables, sensitivity analysis and real-time control," *J. Comput. Appl. Math.*, vol. 120, nos. 1–2, pp. 85–108, Aug. 2000.